



Surface interaction of tetrabromobisphenol A, bisphenol A and phenol with graphene-based materials in water: Adsorption mechanism and thermodynamic effects

Hepsiba Niruba Catherine^{a,b}, Kok-Hou Tan^a, Yang-hsin Shih^{a,*}, Ruey-an Doong^c, Basavaraj Manu^b, Jiann-yuan Ding^d

^a Department of Agricultural Chemistry, National Taiwan University, Taipei, 106, Taiwan

^b Department of Civil Engineering, National Institute of Technology Karnataka, Surathkal, 575025, India

^c Department of Biomedical Engineering and Environmental Sciences, National Tsing Hua University, Hsinchu, 30013, Taiwan

^d Center of General Education, Wenzao Ursuline University of Languages, Kaohsiung, 80793, Taiwan

ARTICLE INFO

Keywords:

Emerging contaminants
Phenol
Bisphenol A
Tetrabromobisphenol A
Graphene oxide
Temperature
Sorption

ABSTRACT

Carbon-based materials, especially graphene nanocomposites (GNS) have attracted wide attention in recent years. In this study, graphene oxide (GO) and reduced graphene oxide (rGO) were prepared using the Improved Hummers method and were investigated for their adsorption behavior of emerging contaminants such as tetrabromobisphenol A (TBBPA), bisphenol A (BPA), and a conventional contaminant, phenol. The adsorption capacity seemed to slightly increase with increasing reduction degree of GO, highlighting its hydrophobic effect. The adsorption kinetics and isotherms were well delineated using pseudo-second-order and Langmuir equations respectively. At higher temperatures, the adsorption of these selected organic contaminants on GO and rGO slightly increased, also indicating the slight effect of temperature on the adsorption in the environment. From a thermodynamic analysis, the endothermic and spontaneous reaction was observed. The adsorption mechanisms included hydrophobicity, π - π interactions and π electron acceptor and donor ones. GNS can suspend in water even after adsorbing pollutants at the water interface. This would enhance the transport of these contaminants with nanomaterials in the environment. These findings are valuable to elucidate the interaction mechanism between phenol, BPA, and TBBPA on GNS while further understanding the physicochemical behavior of these organic contaminants in the environment.

Summary: Adsorption capacities of emerging contaminants, BPA and TBBPA, as well as phenol on graphene oxide (GO) and reduced GO (rGO), were similar. Higher temperatures slightly increased the adsorption of these phenolic compounds on GO and rGO, which also indicated an endothermic and spontaneous process.

1. Introduction

The removal of emerging contaminants (ECs) has become an important issue in environmental pollution and water purification systems. ECs are a group of compounds that include pesticides, pharmaceuticals, and flame retardants (Puga et al., 2020). These substances are of concern worldwide due to their impact on human health and the environment. Two ECs, bisphenol A (BPA) and tetrabromobisphenol A (TBBPA), are chosen in this study since they have been widely measured in the environment (Yang et al., 2015; Waiyarat et al., 2022). Another target compound is phenol since it has the elementary chemical of the two emerging compounds, has been listed as a priority pollutant by various

environmental agencies, and is also classified as a hazardous pollutant due to its potential risk to human health and toxicity to aquatic life (ECHA, 2022).

Conventional wastewater treatment plants are not always effective in the removal of these ECs since EC removal efficiencies typically range from 20-50% during primary treatment, 30-70% in systems that include primary and secondary treatment, and over 90% in systems that reach tertiary treatment (Rout et al., 2021). Although various treatment methods have been investigated (Wang et al., 2013), adsorption remains to be the most efficient and economical method for treating pollutants (Kwon and Lee, 2015; Zhang et al., 2018). Previously, we studied sorption kinetics and thermodynamics of organic contaminants in activated

* Corresponding author.

E-mail address: yhs@ntu.edu.tw (Y.-h. Shih).

carbon (Shih and Gschwend, 2009), carbon nanotubes (Li et al., 2017; Shih and Li, 2008), black carbon (Shih et al., 2012a; Su et al., 2018). Recently, researchers have reported that the adsorption of organic compounds with various carbonaceous materials follow different mechanisms due to their pore structures and functional groups (Liu et al., 2020). Efficient removal of TBBPA by biochar and activated carbon was proposed by Li et al. (2020) and Liu et al. (2019), respectively. Supong et al. (2019) used activated carbon to remove bisphenol A by adsorption.

Nanomaterials are considered to be on the cutting edge of material science research and have been applied in various fields including life science, energy, and environmental applications since the introduction of the term “nanotechnology” by Richard Feynman in 1959 (Bayda et al., 2019). Due to the rapid development of nanotechnology, nanoscale carbon-based materials such as graphene have been gaining attention worldwide (Mauter, 2008; Ren and Cheng, 2014). They have widespread applications and also perform as adsorbents, transistors, sensors (Deng et al., 2012), supercapacitors (Huang et al., 2012), and drug carriers (Dhinakaran et al., 2020). A newer member of carbon-based materials, graphene nanomaterials (GNS) that include graphene oxide (GO) and reduced graphene oxide (rGO), in recent years, have received much attention in nanotechnological applications, including their efficient use in the adsorption of various environmental pollutants (Kozlov et al., 2012; Yan et al., 2014; Tene et al., 2022). GNS shows excellent performance in the adsorption of organic contaminants that include PAHs (Shen et al., 2015; Sreeprasad and Pradeep, 2012) and their derivatives, pesticides, dyes, phenolic compounds, and antibiotics (Jin et al., 2015; Neelaveni et al. 2019; Xu et al., 2012; Zhang et al., 2014). The main feature of the material that contributes to its outstanding performance is the presence of sp^2 hybridized nano-carbons. The presence of an ample amount of adsorption sites, its flat structure, defects, wrinkles and oxygen-carrying functional groups on the structure makes the material a promising adsorbent.

The large-scale production and usage of GNS in biomedical, electronic, and energy sectors, with a market size of USD 2,172.2 million in 2022, have led to its release into the environment with unknown implications (Fortune Business Insights, 2022; Louie et al., 2016). Besides the large-scale production and usage of GO, most of the GO that is found in the environment exists in the reduced form; recent reports show that GO can be reduced to rGO independently by both sunlight and bacterial degradation (Dimiev et al., 2013). GO could suspend well in water due to its electrostatic repulsion with carboxyl and hydroxyl groups, while rGO suspension depends on its type and distribution of oxygen functional groups based on the reduction approaches used (Qi et al., 2016); however, their colloidal stability in water also depends on water chemistry such as pH, ionic strength, natural organic matters, etc. (Chowdhury et al., 2013; Chowdhury et al., 2015; Goodwin et al., 2018). It is important to understand the adsorption of pollutants at the GNS-water interface to assess the adsorption capacity and also its environmental impact. The ability of GNS as a strong adsorbent can enhance the adsorption of organic pollutants on the interface and, followingly, its transport in water (Lu et al., 2018). Once GNS are released into the environment, their adsorption along with the organic pollutants will influence their fate in the environment (Dai et al., 2022).

In this study, GO and rGO we synthesized were used as adsorbents to investigate the adsorption of three aromatic compounds: TBBPA, BPA, and phenol. The effect of adsorption kinetics, isotherms, and thermodynamic analysis of these phenolic compounds on GO and rGO in aqueous solutions were investigated. Furthermore, the interaction of organic compounds on GO and rGO was evaluated both experimentally and spectroscopically. A better understanding of the adsorption of these organic contaminants with graphene-based materials will help not only in water treatment but also in the prediction of the fate and risk of these contaminants in the environment.

2. Experimental

2.1. Materials and reagents

Graphite flakes (<20 mm) and potassium permanganate ($KMnO_4$) were purchased from Sigma-Aldrich. Hydrochloric acid (HCl, 37%), sulfuric acid (H_2SO_4 , 98%), and phosphoric acid (H_3PO_4 , 85%) with Grade AR were purchased from Merck. Phenol, BPA, and TBBPA were obtained from Acros chemical company. Hydrogen peroxide (30–32%) Grade AR was purchased from Acros. All solutions were prepared using deionized (DI) water (Millipore, Temecula, CA, USA).

2.2. Synthesis of GO and rGO

GO was synthesized by the Improved Hummers method (Sahu et al., 2017). In brief, 2.0 g of graphite flakes were added to a mixture of 225 mL of sulphuric acid and 25 mL of phosphoric acid and maintained at a temperature of 35°C. 5.0 g of potassium permanganate was gradually added to the solution maintained at 35°C and stirred continuously for 10 hrs. The resultant mixture was cooled in an ice bath, diluted with 225 mL of DI water, and then 3 mL of 30% hydrogen peroxide was added to the mixture to remove the residual permanganate. A large number of bubbles were released, and the solution color changed to a brilliant yellow. The suspension was centrifuged several times and washed with 0.1 N hydrochloric acid and phosphate buffer to remove extra manganese ions. The final solution was washed with DI water to lower the pH value to around 5-7 and then dried in a rotary vapor at 45°C. The GO suspension was prepared by sonication of GO sheets in DI water for 2 hrs.

The thermal reduction of GO was performed in a quartz tube furnace, in which GO was placed in an aluminum boat placed inside the quartz tube in the presence of argon gas at 400 ° C for 4 hrs. The graphene oxide was thermally expanded and reduced to obtain reduced graphene oxide (rGO) in powder form (McAllister et al., 2007).

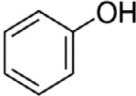
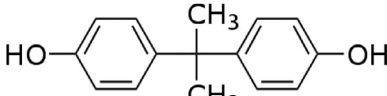
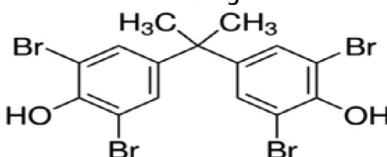
2.3. Characterization of graphene-based materials

The surface morphological characterization was performed by using scanning electron microscopy (SEM, JOEL JSM-7600F) and transmission electron microscopy (TEM, JEOL JEM-200CX). SEM/TEM images of the GO and rGO were captured digitally for further size analysis. The properties of the GO and rGO samples were characterized by Fourier-transform infrared spectroscopy (FTIR), Raman spectroscopy, and X-ray diffraction (XRD) at different beamlines at the National Synchrotron Radiation Research Center (Taiwan). The surface elemental composition was also accomplished by using Energy Dispersive X-ray (EDX) analysis. For the specific surface area (SSA) of the synthesized GO and rGO, N_2 adsorption-desorption experiments were carried out. The electrophoretic mobility of GO samples at different pH values was measured by Zetasizer Nano ZS dynamic light scattering (DLS, Malvern, MA), and their zeta potentials were calculated according to the Helmholtz-Smoluchowski equation.

2.4. Adsorption experiments

The physicochemical properties of the pollutants considered in our study were listed in Table S1. Adsorption experiments were performed in a batch approach to determine the kinetics and isotherms for TBBPA, BPA, and phenol adsorption by GNS (Ji et al., 2013). Briefly, TBBPA, BPA, and phenol were dissolved in a background solution (0.01 M $CaCl_2$ in DI water and 200 mg/L NaN_3), respectively. $CaCl_2$ is used to maintain the ionic strength and NaN_3 acts as a bio-inhibitor. Each chemical solution at a different initial concentration was mixed with an adsorbent (rGO and GO of fixed amount 5 mg) in 4 mL amber vials with PTFE screw caps and then placed on a shaker at 150 rpm for 24 hrs in the dark to reach equilibrium.

Table 1
Molecular structure and chemical properties of phenolic compounds.

Compound	Structure	K_{ow}	pK_a	Solubility (g/L)
Phenol		1.16	10	86.6
BPA		3.36	9.6	0.03
TBBPA		4.5	7.5/8.5	0.004

All experiments were carried out in triplicate, including using blanks, and the standard error was less than 5%. The pH values of the sample before and after the experiments remained the same at around pH 6. Kinetic studies were performed by using 20 mg/L sorbates and 5 mg of GO or rGO in the capped vials. Due to the lowest solubility of TBBPA, the aqueous concentration around its solubility in Table 1 was used. The suspension was shaken to determine the equilibrium time at an interval of 15 min to 24 hrs. The experiments for isotherms at different temperatures were performed by adding various concentrations of sorbate and shaking for more than 48 hrs at 15, 25 and 35°C to determine the thermodynamic behavior of the system. The aqueous samples were collected to determine the chemical concentration. The concentrations of TBBPA, BPA, and phenol in the supernatants were immediately analyzed by using high-performance liquid chromatography (HPLC, Agilent 1200) equipped with a C8 column (5 μ m, 4.6 \times 150 mm) and UV/Vis detector. The details of the HPLC parameters were listed in Table S1.

2.5. Data analysis

The adsorption capacity (Q_e , mg/g) is calculated using the following Eq. (1)

$$Q_e = (C_0 - C_e)V/M \quad (1)$$

where C_0 and C_e are the initial and final concentrations of the compound, respectively; V is the aqueous volume in the vial (mL); and M is the mass of the adsorbent used in the experiments (mg).

Pseudo-first-order and pseudo-second-order kinetic models were used to analyze the adsorption kinetics of these phenolic compounds on two graphene-based materials in Eqs. (2) and (3).

$$\ln(Q_e - Q_t) = \ln Q_e - k_1 t \quad (2)$$

where Q_t (mg/g) is the adsorbed amount of sorbate onto the adsorbent with time, k_1 (min^{-1}) is the pseudo-first-order rate constant, and t (min) is time. The values of k_1 and Q_e were calculated from the linear plots of $\ln(Q_e - Q_t)$ versus t . The pseudo-second-order model can be expressed as

$$\frac{t}{Q_t} = \frac{1}{k_2 Q_e^2} + \frac{1}{Q_e} t \quad (3)$$

where k_2 (g/mg min^{-1}) is the pseudo-second-order rate constant.

Two nonlinear models, Langmuir and Freundlich equations, were utilized to describe the fitting of the adsorption isotherm of the three chemicals on graphene-based materials Eq. (3) and (4)

$$Q_e = \frac{bq_m C_e}{1 + bC_e} \quad (4)$$

$$Q_e = K_f C_e^{1/n} \quad (5)$$

where C_e (mg/L) is the equilibrium concentration of sorbate in the solution, b (L/mg) is a coefficient in the Langmuir equation, q_m (mg/g) is the Langmuir monolayer adsorption capacity, K_f is Freundlich adsorption constant, and n is exponential Freundlich coefficient.

The Gibbs free energy change (ΔG , kJ/mol) was calculated by the Van't Hoff equation (where R is the universal gas constant 8.314 J/mol K) shown in Eq. (6):

$$\Delta G = -RT \ln(K_c) \quad (6)$$

where T is the temperature (K), and the equilibrium constant (K_c) equals Q_e/C_e at a specific temperature.

Information on the inherent energetic changes related to the adsorption is also provided by further thermodynamic analysis. According to the Gibbs-Helmholtz Eq. (7), the change in enthalpy (ΔH , kJ/mol) and the change in entropy (ΔS , kJ/mol K) under constant temperature were calculated.

$$\Delta G = \Delta H - T\Delta S \quad (7)$$

3. Results and discussion

3.1. Characterization of graphene-based materials

The surface morphology and microstructure of GO and rGO are illustrated in SEM and TEM images (Fig 1 a-d). Both GO and rGO displayed wrinkles and crumpled features that indicate the nature of graphene. They are also associated with the presence of sp^3 sites of oxygen functionalities and structural defects in the basal plane of the GO nanosheet. The SEM micrograph shows that rGO (Fig. 1b) has an irregular exfoliated structure and an increase in folds (Wang et al., 2014a). TEM images of GO and rGO (Fig. 1c and d) show the surface of GO is flat with wrinkles located at the edges, whereas for rGO, they are located at the basal planes, forming groove regions (Gupta and Khatri, 2017). The results of the elemental analysis of the GO and rGO by SEM/EDX are presented in Table 2. The C content was 53% for GO and 80% for rGO, while the ratio between the atomic percentages of oxygen to carbon (O/C) indicates a higher polarity of GO than rGO, which is consistent with their nature. The SSA of the synthesized GO and rGO was 1.10 m^2/g and 228 m^2/g , respectively. The specific surface area for GO was much lower compared to that of rGO, which could be due to the formation of bulk graphene oxide with long-range array and incomplete exfoliation (Jiang et al., 2016).

XRD was employed to characterize the formation of GO and rGO from graphite (Fig. 2a). The presence of intense peaks of graphite ($2\theta=26.5$), rGO ($2\theta=24.6$), and GO ($2\theta=10.1$) in their respective spectra clearly indicate the materials that we synthesized were in good agreement with the literature data (Mishra et al., 2014). After the oxidation

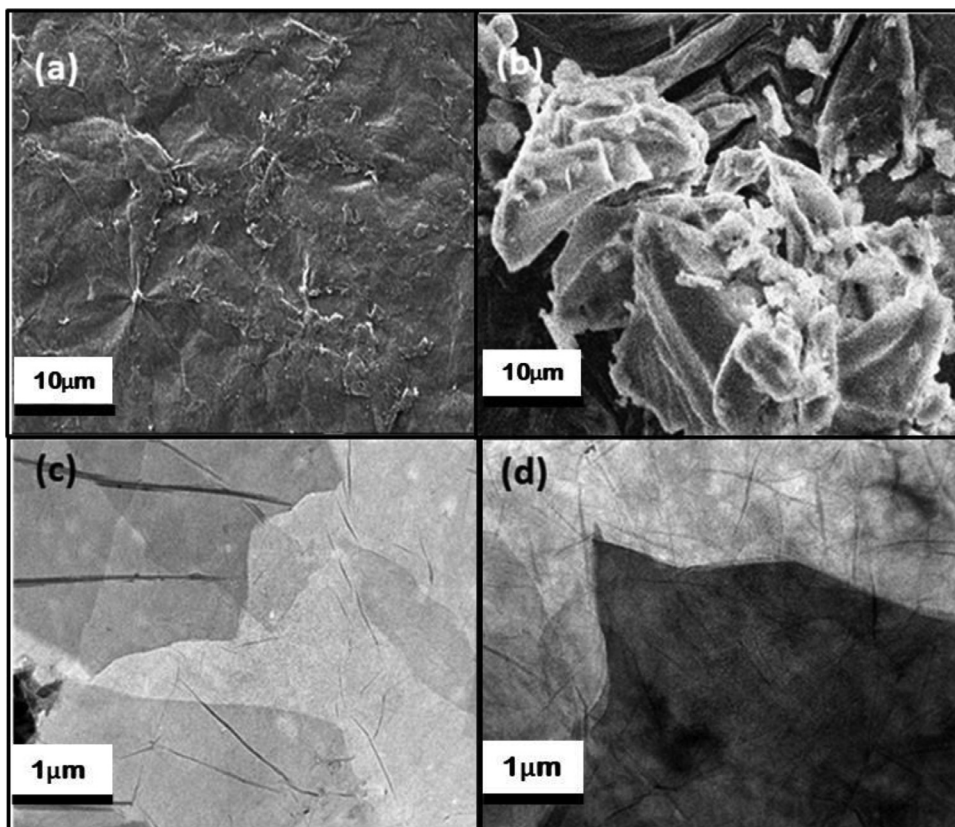


Fig. 1. SEM images of (a) GO and (b) rGO. TEM images of (c) GO and (d) rGO.

Table 2
Selected physicochemical properties of carbonaceous materials.

Carbonaceous materials	Elemental composition ^a			SSA(m ² /g) ^b	I _D /I _G ^c
	C	O	O/C		
GO	53	42	0.79	1.10	0.93
rGO	80	16	0.20	227.82	1.01

^a Analyzed using Energy-dispersive X-ray spectroscopy.

^b Specific Surface Area measured using the Brunauer–Emmett–Teller (BET) method.

^c Intensity at D to intensity at G band analyzed with Raman spectrometry.

of graphite, the strong (002) peak at 26.5° ($d_{002}=0.336$ nm) vanished and a new (001) peak appeared at 10.1° ($d_{001}=0.875$ nm). After the reduction of GO, the peak shifted back to 24.6° , indicating a decrease in the number of C-O bonds and a shortening of interplanar distance.

FTIR spectra were examined for the surface O-containing functional groups in GO, rGO, and graphite (Fig. 2b). The FTIR results for GO show a broad peak at 3380 cm^{-1} due to O-H stretching, and the other peaks located at 1735 cm^{-1} , 1624 cm^{-1} , 1225 cm^{-1} and 1060 cm^{-1} could be attributed to stretching vibrations of carbonyl C=O, carboxyl O=C-O, epoxy C-O-C, and alkoxy C-O bonds, respectively (Jiang et al., 2015; Pei et al., 2013). Compared to GO, the spectrum of rGO has very few O-containing functional groups on its surface. Besides that, rGO shows a decrease in the peak intensities at 3380 cm^{-1} , 1225 cm^{-1} , and 1735 cm^{-1} , indicating the loss of OH, epoxy and carbonyl groups (Kumar et al., 2014).

The Raman spectra (Fig. 2c) show the appearance of two prominent peaks of G bands (1607 and 1595 cm^{-1}) and D bands (1363 and 1354 cm^{-1}) for GO and rGO ensuring the confirmation of lattice distortions. There is a shift in the G band for GO to a higher wavenumber due to the oxygenation of graphite resulting in the formation of sp^3 carbon atoms, whereas the broadened D band is due to the reduction in the size of the

sp^2 domain. The D band is related to the vibration of carbon atoms with the bonds related to the carbon network, while the G band is related to the E_{2g} vibration mode of sp^2 carbon domains. The I_D/I_G ratio is used to measure the defect levels in the graphitic system (Table 2). The ratio is higher for rGO (1.01) compared to GO (0.93) due to the decrease in the average size of sp^2 domains that were newly formed during the reduction (Perumbilavil et al., 2015).

Zeta potential was used to find out the stability of rGO and GO and also served as an indicator to identify their dispersion stability. Nanofluids whose zeta potential values range from ± 30 to 40 mV are considered stable (Kamatchi et al., 2015). The zeta potential values of both GO and rGO decreased with increasing pH and rebounded after reaching a minimum value. Fig. 2d shows the value for GO is -45 mV at pH 9 and the value for rGO is -32 mV at pH 8. GO was stable over a wide range of pH due to the presence of strong electrostatic repulsions (Lu et al., 2018), while rGO is unstable in water at pH values other than pH 8.

3.2. Adsorption kinetics of TBBPA, BPA, and phenol on GO and rGO

The adsorption kinetics of TBBPA, BPA, and phenol on GO and rGO is shown in Fig. 3. The adsorption of these chemicals on GO showed rapid adsorption in the first 60 min, then followed a slow pattern for up to 200 min, and finally reached equilibrium at 480 min. As shown in Fig 3b for rGO, adsorption rapidly increased in the first 5 min and adsorption equilibrium was reached in 120 min, similar to other literature (Wang et al., 2014b). A slightly higher adsorption amount of these compounds was observed for rGO compared to GO, in which a maximum adsorption capacity of 35 mg/g was achieved by rGO and 25 mg/g by GO for TBBPA. This could be due to the large surface area of rGO and its sheet-like structures mentioned in the literature (Yu et al., 2017).

The kinetic results were fitted by two models: pseudo-first-order and pseudo-second-order kinetics. The correlation coefficient (R^2) and the rate constants for each chemical were determined (Table S2). Strong R^2 regressions (0.88-0.99) were observed using both pseudo-first-order and

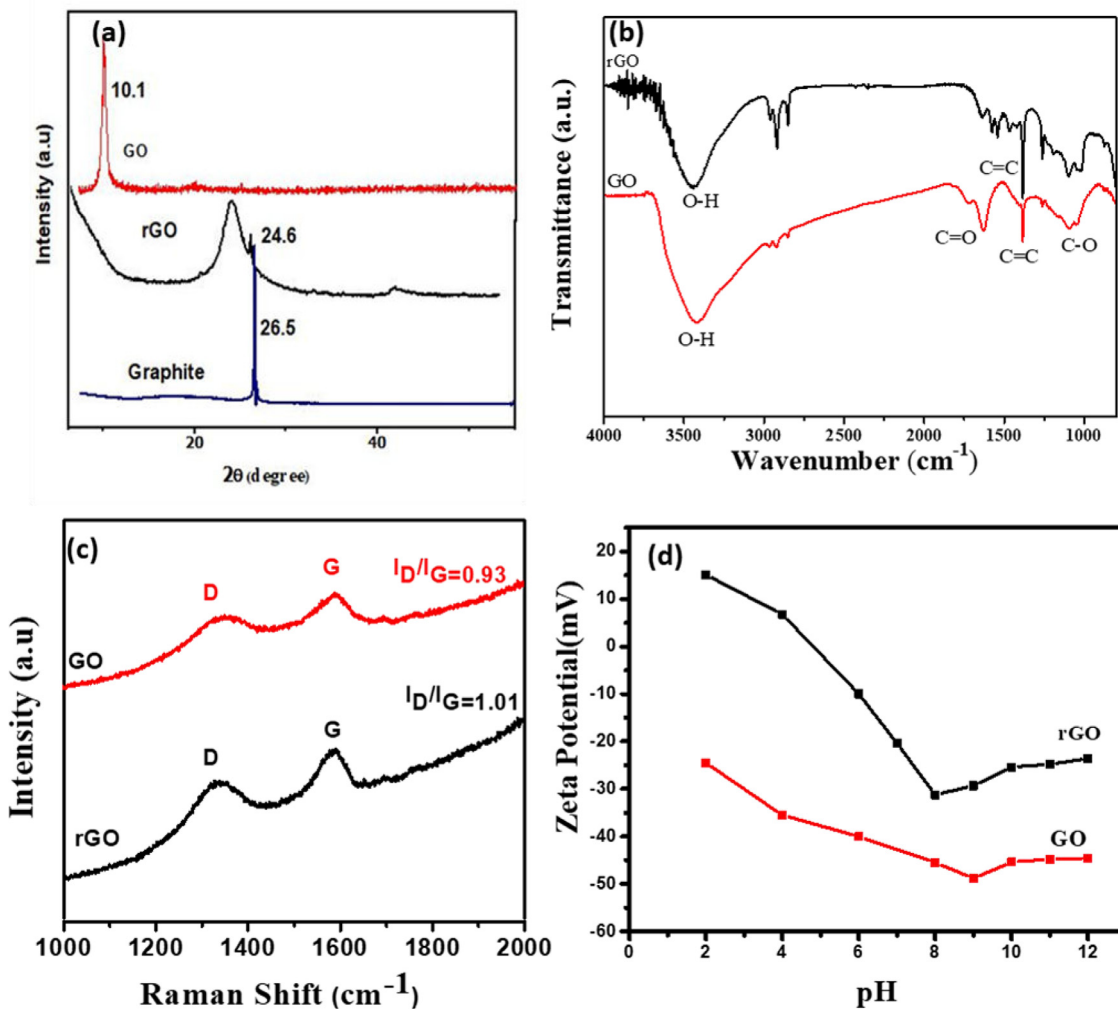


Fig. 2. The (a) XRD, (b) FTIR, and (c) Raman spectra of graphite, rGO, and GO, and the (d) Zeta potentials of GO and rGO.

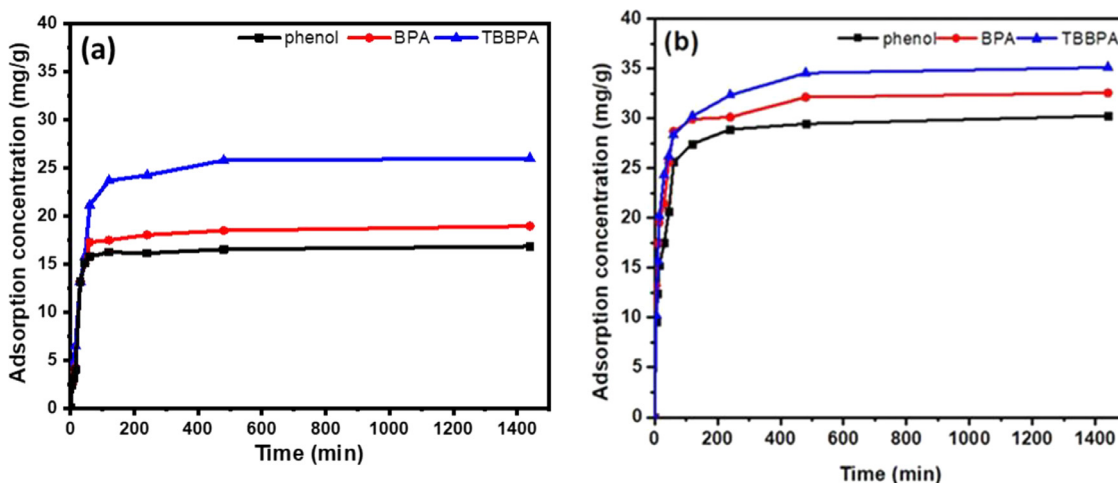


Fig. 3. Adsorption kinetics of (a) phenol, BPA and TBBPA on GO and that of (b) phenol, BPA and TBBPA on rGO.

pseudo-second-order kinetic models, but a better fit was observed for the pseudo-second-order kinetic model, suggesting that the sorption of TBBPA, BPA, and phenol onto these adsorbents depends on the amount of the solute adsorbed on the surface of the adsorbent and the amount adsorbed at equilibrium (Bele et al., 2016). The adsorption rate constant k_2 estimated using the pseudo-second-order kinetic model was higher

for rGO (11.7, 10.5, 12.2 g/mg min⁻¹ for phenol, BPA, and TBBPA, respectively) than GO (2.22, 9.87, 5.64 g/mg min⁻¹), thus confirming that rGO exhibited faster adsorption kinetic than GO (Kwon and Lee, 2015). The fast adsorption of rGO has been previously highlighted by its powerful adsorption towards dyes, nitroaromatic and ECs (Minitha et al., 2017; (Chen and Chen, 2015; Jin et al., 2015). This observation can be

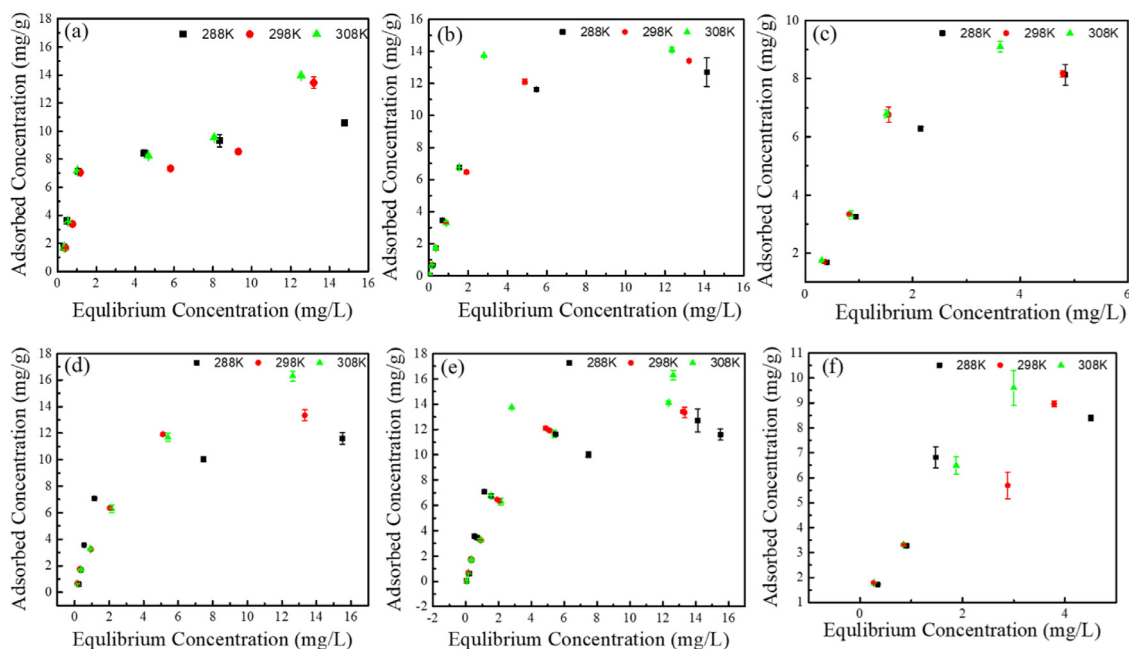


Fig. 4. Adsorption isotherms of (a) phenol, (b) BPA (c) TBBPA on GO and (d) phenol, (e) BPA, (f) TBBPA on rGO under different temperature conditions.

attributed to the higher hydrophobicity of the rGO surface, which allows the hydrophobic phenyl ring of sorbates to approach its surface easily with little electrostatic repulsion. In contrast, GO with a larger number of polar carbonyl and carboxyl groups requires phenolic sorbates to approach its surface at a specific orientation for adsorption, hence proceeds at a slower pace.

3.3. Adsorption isotherms of TBBPA, BPA, and phenol on GO and rGO

3.3.1. Effect of initial concentration

The adsorption of the three single compounds on GNS was studied at various initial concentrations at 288K, 298K, and 308K. In Fig. 4a and d, when the phenol concentration was around 15 mg/L at 288K, its adsorption concentration on both GO and rGO reached 10.5 mg/g and 11.8 mg/g. Adsorption isotherms of TBBPA on GO and rGO had a similar pattern while adsorption of BPA is slightly higher on GO than on rGO. As expected, the uptake of phenol, BPA, and TBBPA on GO and rGO increases with increasing initial concentration and eventually reaches equilibrium, which was also observed by Wu et al. (2016).

Langmuir and Freundlich models were employed to gain insight into the adsorption behavior. The fitting parameters of Langmuir and Freundlich models of phenol, BPA, and TBBPA on GO and rGO are listed in Table S3. The results show that the studied adsorption reactions fit better in the Langmuir model than in the Freundlich model. The Langmuir monolayer adsorption capacity of rGO is larger than GO for BPA and TBBPA, but smaller than GO for phenol, indicating that rGO is more efficient in adsorbing less polar molecules. On the contrary, GO performs better in isolating molecules with higher polarity. More π - π interactions between the aromatic structure of the compound and sp^2 regions of rGO could contribute to a higher adsorption capacity of BPA and TBBPA in rGO than in GO. Furthermore, as shown in Table S3, the maximum adsorption capacities (q_m , mg/g) of BPA on GO and rGO in the Langmuir model are 20.98 and 23.20 mg/g at 308 K, respectively, which are slightly higher than those of phenol and TBBPA. Since the adsorption isotherms of phenol, BPA, and TBBPA on GO and rGO fitted better in the Langmuir model than in the Freundlich model, it was suggested that the adsorption behavior of these reactions is governed by monolayer adsorption on the surface. The results were compared with different carbon-based materials reported in the literature for the com-

parison of TBBPA, BPA, and phenol and summarized in Table 3. In general, the adsorption activity of the GO and rGO sample in this work was found to be lower than those reported: the GO and rGO prepared by Wang et al. (2018) had a slightly higher phenol adsorption capacity (25.5 mg/g and 45.5 mg/g) than ours did due to different preparation methods. Meanwhile, the rGO prepared by Rout and Jena (2022) and a commercial powdered activated carbon used by Xie et al. (2020) demonstrated significantly higher phenol adsorption, a result that can be attributed their larger surface area. After normalizing the SSA found in these papers, our GO and rGO were determined to have the highest adsorption capacity per unit of surface area (Table 3).

In Table 3, the adsorption of BPA was reported to range from 15.7 mg/g to 356 mg/g with rGO which adsorbs more BPA than GO. Meanwhile, the adsorption capacity of TBBPA has a narrower range between 87.0 mg/g to 116 mg/g. Furthermore, during our experiments, GO and rGO suspended well in water in the presence of 10 mM $CaCl_2$. These results demonstrate that GNS can adsorb organic compounds and simultaneously suspend well in water, affecting the aquatic environment by extending the expense of organic contaminants in the environment through the adsorption on GNS.

3.3.2. Effect of temperature

The adsorption isotherms of phenol, BPA, and TBBPA on GO or rGO were also studied under different temperatures. In Fig. 4, compared to 288K, the maximum adsorption of phenol and BPA on GO (Fig. 4a and 4b) and rGO (Fig. 4c and 4d) at around 12 mg/L was higher at 298 K and 308 K. The Langmuir model could also be employed to describe these isotherms to understand the adsorption thermodynamic behavior (Table S3). Since the adsorption capacity of phenol and BPA increased with an increase in temperature, it is indicated that higher temperatures are suitable for phenol and BPA adsorption on GO and rGO. Notably, the adsorption of GO on TBBPA increased slightly with increasing temperature. Contrary to the observation in phenol and BPA adsorption, the adsorption capacity of rGO decreased with increasing temperature, supporting the conclusion that the interaction between rGO and TBBPA is mainly governed by the weak π - π interactions between the aromatic structure of the compound and sp^2 regions of rGO. These interactions, which have a calculated interaction energy of -13.497 kcal/mol (56.471 kJ/mol) (Ghahghaey et al., 2021), could be easily overcome when en-

Table 3
Adsorption properties of phenol, BPA and TBBPA on GO, rGO, and some carbonaceous materials, ^b

Pollutant	Adsorbent	Loading (g/L)	T (K)	t (h)	pH	q _m (mg/g) ^a	q _m /SSA	Reference
Phenol	rGO	0.4	303	1.25	8	602.41	-	Rout and Jena, 2022
	GO	0.04	298	1	7	25.5	-	Wang et al., 2018
	rGO	0.04	298	1	7	45.5	-	Wang et al., 2018
	AC (Commercial)	0.63	298	7	5	246.3	0.24	Xie et al., 2020
	GO	1.25	308	4	6	19.2	17.5	This work
BPA	rGO	1.25	308	8	6	16.1	0.07	This work
	GO	0.04	298	1	7	91.3	-	Wang et al., 2018
	rGO	0.04	298	1	7	356.1	-	Wang et al., 2018
	GO	0.06	298	0.5	8	49.3	-	Phatthanakittiphong and Seo, 2016
	AC (Biomass)	4.00	298	1.33	7	15.7	0.02	Supong et al., 2019
TBBPA	GO	1.25	308	4	6	21.0	19.1	This work
	rGO	1.25	308	8	6	23.2	0.10	This work
	GO	0.02	298	10	6	115.8	-	Zhang et al., 2013
	MGAC	0.15	293	10	9	110.7	0.13	Liu et al., 2019
	Biochar	0.1	303	24	7.5	87.0	-	Li et al., 2020
	GO	1.25	298	4	6	17.3	15.7	This work
	rGO	1.25	288	8	6	14.8	0.06	This work

^a q_m: Maximum adsorption capacity.^b SSA: Specific surface area.**Table 4**
Adsorption thermodynamic parameters for phenol, BPA and TBBPA on rGO and GO

Adsorbent	Compound	ΔG (kJ/mol)			ΔH (kJ/mol)	ΔS (J/(K mol))
		288 K	298 K	308 K		
GO	Phenol	-18.86	-19.11	-20.38	6.09	0.07
	BPA	-18.58	-18.86	-18.95	5.82	0.08
	TBBPA	-19.08	-20.18	-21.21	11.84	0.10
rGO	Phenol	-19.03	-19.78	-20.51	2.25	0.07
	BPA	-18.66	-18.83	-18.93	4.19	0.07
	TBBPA	-19.54	-20.08	-21.28	1.09	0.08

ergy is supplied with increasing temperature and, hence, fewer TBBPA molecules would be held on the surface of rGO at high temperatures.

Thermodynamic parameters provide information about the energy changes associated with the adsorption process. The constants listed in Table 4 were determined through linearized data as shown in Fig. 5. From Table 4, the negative ΔG value indicates the thermodynamic feasibility and spontaneous nature of the adsorption process (Ren et al., 2013). At the same interval, the Gibbs free energy was close to the increase in temperature from 288 to 308K, proving that the influence of temperature on the adsorption was insignificant. The decrease in negative ΔG with an increase in temperature implies that higher temperatures favor the adsorption of phenol, BPA, and TBBPA on GO and rGO. Yu et al. (2016) observed a similar sorption pattern in which phenol adsorption on rGO was inversely proportional to the temperature, demonstrating that a higher temperature was effective for the removal of phenol.

The adsorption enthalpies of phenol, BPA, and TBBPA on GO were 6.09, 5.82 and 11.84 kJ/mol, respectively (Table 4). The adsorption enthalpies of phenol, BPA, and TBBPA on rGO were 2.25, 4.19 and 1.09 kJ/mol, respectively (Table 4). The adsorption enthalpies of these compounds on GO were higher than those on rGO, indicating more energy was needed to allow the target molecule to be adsorbed onto the surface of GO than that of rGO. Overall, the ΔH values in the present work lie between 0 and 20 kJ mol⁻¹, suggesting the dominance of physisorption, which was also observed by Wang et al. (2013). Furthermore, the positive values of ΔH indicate that the adsorption process is endothermic in nature (Kyzas et al., 2013). The positive values of ΔS indicate stability in the adsorption process, with minimal structural change at the solid-liquid boundary (Shih et al., 2012). The low positive values of ΔS demonstrate that the randomness is moderately increased during the adsorption process, which relates to the degree of freedom of the adsorbed molecules (Zhang et al., 2013). Together, the slight positive ΔS and endothermic nature are the results of a large quantity of water

displacement from the surface of the adsorbent during the adsorption process (Yu et al., 2017). A positive change in enthalpy and a positive change in entropy have also been observed in a previous study on the adsorption of phenolic compounds on carbon-based material (Dhorabe et al., 2016).

3.4. Adsorption mechanisms of TBBPA, BPA, and phenol on GO and rGO

The adsorption of graphene materials at the molecular level is generally dependent on the structure of the adsorbate and the surface of GNS (Chen et al., 2008). Several mechanism models such as hydrophobic interaction, hydrogen bonding, and electrostatic interaction could be involved in the adsorption of phenolic compounds based on theoretical and experimental results (Chen et al., 2008; Chen and Chen, 2015; Dehmani et al., 2022; Wang et al., 2014). For the three adsorbates tested, only a slight difference in adsorption was found (Fig. 4 and Table S3) and a slightly higher adsorption capacity was observed for rGO compared to GO, highlighting the structural and surface difference between them. For both GO and rGO, adsorption affinity followed the order of BPA>phenol>TBBPA.

From the values of water solubility (C_{sat}) and n-octanol–water partition coefficient (K_{OW}) in Table 1, BPA has a higher hydrophobicity than phenol, which could contribute to the highest adsorption of BPA than phenol on both rGO and GO.

From the FTIR spectra, it was revealed that rGO was more hydrophobic than GO (Fig. 2b). As BPA is hydrophobic, hydrophobic interactions play an important role in its adsorption process. Both rGO and GO used in this study contain electron-rich sites and electron-depleted sites, leading to the delocalization of π electrons (Fagan et al., 2004). Since π-electron can interact with the π-electron of the benzene ring and affect the adsorption capacity of aromatic compounds on graphene-based materials, π-π interactions have been proposed to dominate the adsorption of aromatic compounds on graphene-based materials (Fig. 6a and

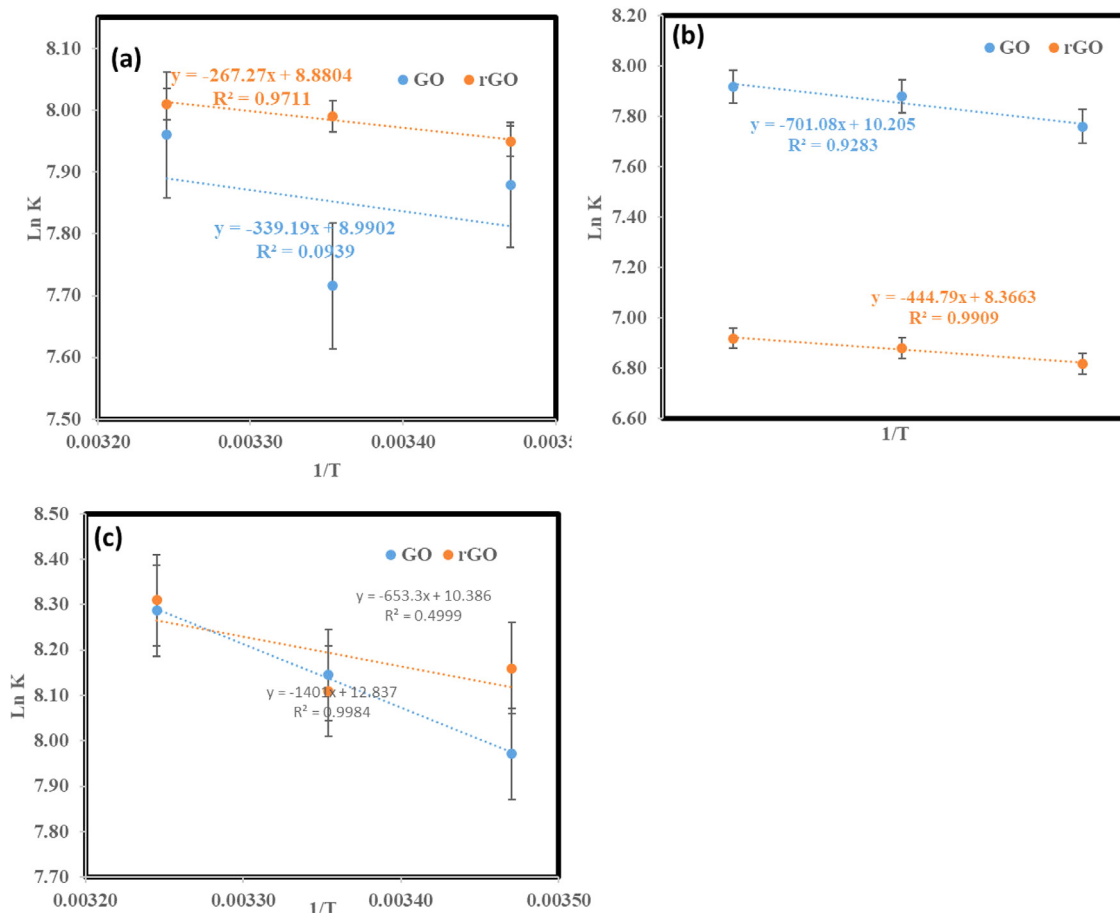


Fig. 5. Plots of ln K versus 1/T for adsorption of (a) phenol, (b) BPA and (c) TBBPA on GO and rGO.

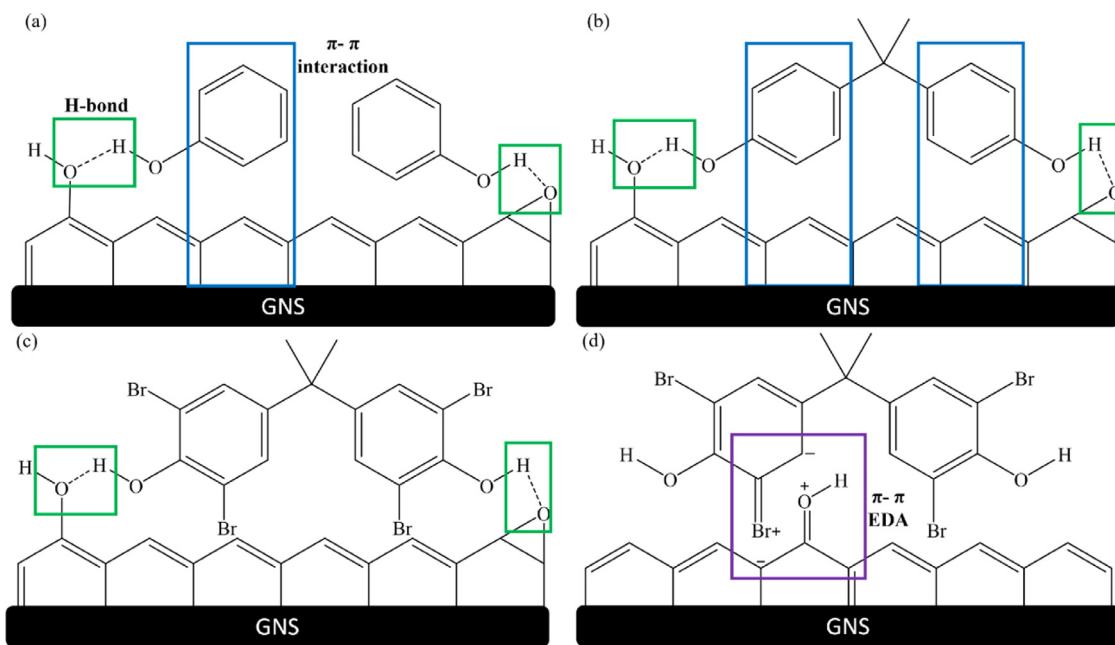


Fig. 6. Adsorption of (a) phenol, (b) BPA, and (c) TBBPA on GNS surface. The interaction between TBBPA and GNS through EDA was demonstrated in (d).

b) (Chen et al., 2007; Yan et al., 2015) and adsorbents with aromatic moieties (Ji et al., 2022; Wu et al., 2020). This explains the higher adsorption capacity of BPA on GO and rGO compared to phenol. However, although TBBPA is the most hydrophobic compound among the three, with the lowest C_{sat} and highest K_{OW} , it did not achieve the highest adsorption. This could be because the surface of GO and rGO are not made up of hydrophobic functional groups alone; they also consist of some hydrophilic moieties. Additionally, the fused aromatic rings of TBBPA are substituted with two -OH groups and two large bromine atoms, which hinder them from forming strong π - π interactions with GO and rGO (Fig. 6c). These chemical and spatial properties have contributed to the low adsorption capacity of TBBPA on GO and rGO (Ji et al., 2013).

The better adsorption capacity of rGO is attributed to there being fewer carboxyl groups in rGO than in GO. The incorporation of oxygen-carrying functional groups could induce hydrogen bonding between the pollutant and the surface of the graphene-based material, while the absence of O-functional groups could possibly lead to the dominance of π - π interactions (Fig. 6a-6c) (Yan et al., 2014). The adsorptive sites available on graphene-based materials measured by FTIR spectroscopy (Fig. 2b) indicated that the edges and surface of GO have abundant oxygen-carrying functional groups, which include O-H, C-O, C=O, and C(O)O, that could make the surface highly hydrophilic, form hydrogen bonding with water molecules, and hinder π - π interactions. The presence of the H-bond is due to the interaction between the hydroxyl group of phenolic compounds with the hydroxyl group of GO and rGO. Since H-bond energies can range from <17 kJ/mol to 167 kJ/mol (MacLeod and Rosei, 2011), depending on the nature of donor and acceptor atoms, they can participate in the physisorption process. It was considered that this mechanism played an important role in the adsorption of phenolic compounds in our study. These hydrophilic surface functional groups also accounted for the poorer adsorption of aromatic pollutants on GO compared to rGO. Having fewer oxygen-carrying functional groups, rGO is more hydrophobic than GO. This is consistent with the finding in previous studies which showed that rGO is more hydrophobic than the starting material (Kwon and Lee, 2015; Li et al., 2016). Similar results have been observed for the adsorption of phenol on rGO by computational approaches (Yu et al., 2017). In addition to stronger π - π interactions, the electron-rich benzene ring of aromatic pollutants can also interact with the partially positively charged groups of rGO and enhance its adsorption capacity.

On the other hand, GO shows both π electron acceptor and donor (EDA) properties due to the presence of π -electron rings and functional groups (Fig. 6d). It was also reported that π - π EDA interactions would lead to the strong adsorption of hydroxyl-substituted compounds on carbon nanotubes (Chen and Chen, 2015). The π - π interactions between π electron-rich regions present on the graphene layers and electron acceptor substances have been widely used to address the adsorption of organic compounds on the graphene surface: the hydroxyl group (-OH) can result in electron conjugation with the benzene rings, thus making them electron rich.

The value of the adsorption coefficient K_d (L/kg), calculated by dividing the adsorbed amount (q_e) by the equilibrium concentration (mg/L), is presented in Fig. S1. The results indicated that the adsorption of all pollutants decreased with increasing equilibrium concentration, which is in agreement with the adsorption behavior of nitroaromatic compounds and phthalic acid esters on GNS (Chen and Chen, 2015; Lu et al., 2018). It is noted that the values of K_d of phenol and BPA were almost overlapping when the concentration increased.

The q_{max} value of BPA, phenol, and TBBPA adsorption on rGO appears to negatively relate to their molecular sizes, which could be a size exclusion effect on the adsorption of these compounds on rGO. Such a phenomenon was also reported in the PAH adsorption on carbon-based materials as the pore-filling mechanism dominated the adsorption of these compounds (Wang et al., 2014). Although there was slightly higher adsorption of pollutants on rGO than on GO, the SSA normalized adsorption coefficients of rGO could be around 10 times smaller

than those of GO since the SSA of rGO was 10 times higher than that of GO. This might be a result of the existence of very small pores in rGO that prevent the adsorbates from being adsorbed. Overall, the main mechanisms governing the different adsorption of aromatic compounds on GO and rGO include H-bonding, π - π , van der Waals, electrostatic interactions, and hydrophobic interactions.

3.5. Environmental implication of GO and rGO with organic contaminants

The fate of environmental transport of nanomaterials is governed by their colloidal stability (Yan et al., 2015). The stability of many nanomaterials, including metal oxide nanoparticles, was studied in our previous papers (Liu et al., 2012; Peng et al., 2017; Peng et al., 2015; Shih et al., 2012b; Shih et al., 2012c; Tso et al., 2010) and Dai et al. (2022), and GOs (Babakhani et al., 2018; Chowdhury et al., 2013; Chowdhury et al., 2015; Gao et al., 2022). Chowdhury et al. (2013) also indicated that GO is stable in the natural aquatic environment and significant aqueous transport of GO is possible but they also depend on water chemistry. In this study, GO prepared by the modified Hummers method was used to demonstrate the interaction between GNS and pollutants when they enter environmental water. rGO was synthesized to evaluate the potential impact that arose when GNS was left in the environment for a prolonged period and eventually reduced by sunlight or bacteria. GO has a good stability in water for a period of 70 days due to the presence of hydrophilic functional groups (Catherine et al., 2018). Our findings on the dispersion stability of GO using zeta potential measurements (section 3.1) is well supported by the study of Chowdhury et al. (2015), which demonstrated that GO remains stable from pH 4 to 10. In contrast, rGO can only suspend in water at pH 8 (Fig. 2d). Hence, GO is prompt to affect the aquatic ecosystem while rGO has a higher potential to sediment and exert a profound impact on habitats at the bottom of water. Current studies confirm that both GO and rGO will interact with the water environment chemically, with the latter interacting more strongly and faster with organic entities. Hence, their presence could be beneficial from the point of water purification. Nevertheless, further evaluation of their toxicological profile is required to determine whether their presence is harmless, or even beneficial to water recycling.

4. Conclusion

GO nanoflakes and reduced graphene oxide that varied in C/O ratio were successfully synthesized via a modified Hummers method and a thermal method, respectively. The adsorption kinetics of phenol, BPA, and TBBPA onto GO and rGO in aqueous solutions were best fitted to a pseudo-second-order model. The adsorption of these phenolic compounds were of monolayer nature with a higher adsorption capacity observed with rGO than for GO. These adsorption processes were spontaneous ($\Delta G = -18.6$ to -21.3 kJ/mol) with a small change in entropy ($\Delta S = 0.07$ - 0.08). Overall, the adsorption of the three phenolic compounds on GO and rGO were endothermic physisorption reactions with a heat of adsorption of 2.3~11.8 kJ/mol. The results of this study suggest that the mechanisms governing the adsorption uptakes are hydrogen bonding and π - π interactions between phenolic compounds and graphene-based adsorbents. This study has provided a better understanding into the adsorption of these emerging contaminants on graphene-based materials for water treatments and also their fate in the environment.

Funding Information

This research is financially supported by the Ministry of Science and Technology in Taiwan and the Ministry of Human Resource and Development in India. The sponsors did not involve in the conduct of the research or preparation of the article.

Declaration of interests

The authors declare that they have no known competing financial interests or personal relationships that could have appeared to influence the work reported in this paper.

Data availability

Data will be made available on request.

Acknowledgment

The authors thank the financial support from the Ministry of Science and Technology in Taiwan. The authors would also like to thank the Ministry of Human Resource and Development in India for supporting Dr. Hepsiba Niruba Catherine.

Supplementary materials

Supplementary material associated with this article can be found, in the online version, at doi:10.1016/j.hazadv.2022.100227.

References

- Babakhani, P., Bridge, J., Phenrat, T., Doong, R.-a., Whittle, K.R., 2018. Aggregation and sedimentation of shattered graphene oxide nanoparticles in dynamic environments: a solid-body rotational approach. *Environ. Sci.* 5 (8), 1859–1872. doi:10.1039/C8EN00443A.
- Bayda, S., Adeel, M., Tuccinardi, T., Cordani, M., Rizzolio, F., 2019. The history of nanoscience and nanotechnology: from chemical-physical applications to nanomedicine. *Mol.* 25, 112. doi:10.3390/MOLECULES25010112, Page 112 25.
- Bele, S., Samanidou, V., Deliyanni, E., 2016. Effect of the reduction degree of graphene oxide on the adsorption of Bisphenol A. *Chem. Eng. Res. Des.* 109, 573–585. doi:10.1016/J.CHERD.2016.03.002.
- Catherine, H.N., Ou, M.H., Manu, B., Shih, Y.hsin, 2018. Adsorption mechanism of emerging and conventional phenolic compounds on graphene oxide nanoflakes in water. *Sci. Total Environ.* 635, 629–638. doi:10.1016/J.SCITOTENV.2018.03.389.
- Chen, W., Duan, L., Wang, L., Zhu, D., 2008. Adsorption of hydroxyl- and amino-substituted aromatics to carbon nanotubes. *Environ. Sci. Technol.* 42, 6862–6868. doi:10.1021/ES8013612/SUPPL_FILE/ES8013612_SI_001.PDF.
- Chen, W., Duan, L., Zhu, D., 2007. Adsorption of polar and nonpolar organic chemicals to carbon nanotubes. *Environ. Sci. Technol.* 41, 8295–8300. doi:10.1021/ES071230H/SUPPL_FILE/ES071230H-FILE002.PDF.
- Chen, X., Chen, B., 2015. Macroscopic and spectroscopic investigations of the adsorption of nitroaromatic compounds on graphene oxide, reduced graphene oxide, and graphene nanosheets. *Environ. Sci. Technol.* 49, 6181–6189. doi:10.1021/ES5054946/SUPPL_FILE/ES5054946_SI_001.PDF.
- Chowdhury, I., Duch, M.C., Mansukhani, N.D., Hersam, M.C., Bouchard, D., 2013. Colloidal properties and stability of graphene oxide nanomaterials in the aquatic environment. *Environ. Sci. Technol.* 47 (12), 6288–6296. doi:10.1021/es400483k.
- Chowdhury, I., Mansukhani, N.D., Guiney, L.M., Hersam, M.C., Bouchard, D., 2015. Aggregation and stability of reduced graphene oxide: complex roles of divalent cations, pH, and natural organic matter. *Environ. Sci. Technol.* 49 (18), 10886–10893. doi:10.1021/acs.est.5b01866.
- Dai, H., Han, T., Cui, J., Li, X., Abbasi, H.N., Wang, X., Guo, Z., Chen, Y., 2022. Stability, aggregation, and sedimentation behaviors of typical nano metal oxide particles in aqueous environment. *J. Environ. Manage.* 316, 115217. doi:10.1016/j.jenvman.2022.115217.
- Dai, H., Han, T., Cui, J., Li, X., Abbasi, H.N., Wang, X., Guo, Z., Chen, Y., 2022. Stability, aggregation, and sedimentation behaviors of typical nano metal oxide particles in aqueous environment. *J. Environ. Manage.* 316, 115217. doi:10.1016/J.JENVMAN.2022.115217.
- Dehmani, Y., Dridi, D., Lamhasni, T., Abouarnadasse, S., Chtourou, R., Lima, E.C., 2022. Review of phenol adsorption on transition metal oxides and other adsorbents. *J. Water Process. Eng.* 49, 102965. doi:10.1016/J.JWPE.2022.102965.
- Deng, S., Tjoa, V., Fan, H.M., Tan, H.R., Sayle, D.C., Olivo, M., Mhaisalkar, S., Wei, J., Sow, C.H., 2012. Reduced graphene oxide conjugated Cu 20 nanowire mesocrystals for high-performance NO 2 gas sensor. *J. Am. Chem. Soc.* 134, 4905–4917. doi:10.1021/JA211683M/SUPPL_FILE/JA211683M_SI_001.PDF.
- Dhinakaran, V., Lavanya, M., Vigneswari, K., Ravichandran, M., Vijayakumar, M.D., 2020. Review on exploration of graphene in diverse applications and its future horizon. *Mater. Today Proc.* 27, 824–828. doi:10.1016/J.MATPR.2019.12.369.
- Dhorabe, P.T., Lataye, D.H., Ingole, R.S., 2016. Removal of 4-nitrophenol from aqueous solution by adsorption onto activated carbon prepared from *Acacia glauca* sawdust. *Water Sci. Technol.* 73, 955–966. doi:10.2166/wst.2015.575.
- Dimiev, A.M., Alemay, L.B., Tour, J.M., 2013. Graphene oxide. Origin of acidity, its instability in water, and a new dynamic structural model. *ACS Nano* 7, 576–588. doi:10.1021/NN3047378/SUPPL_FILE/NN3047378_SI_001.PDF.
- ECHA, 2022. Phenol [WWW Document]. URL <https://echa.europa.eu/brief-profile/-/briefprofile/100.003.303>. (accessed 12.16.22).
- Fagan, S.B., Souza Filho, A.G., Lima, J.O.G., Mendes Filho, J., Ferreira, O.P., Mazali, I.O., Alves, O.L., Dresselhaus, M.S., 2004. 1,2-Dichlorobenzene interacting with carbon nanotubes. *Nano Lett.* 4, 1285–1288. doi:10.1021/NL0493895/ASSET/IMAGES/MEDIUM/NL0493895N00001.GIF.
- Fortune Business Insights, 2022. Graphene market to reach USD 2,172.2 million by 2029. Graphene Industry Striking CAGR of 30.5% During (2022-2029) [WWW Document] URL.
- Gao, Y., Zeng, X., Zhang, W., Zhou, L., Xue, W., Tang, M., Sun, S., 2022. The aggregation behaviour and mechanism of commercial graphene oxide in surface aquatic environments. *Sci. Total Environ.* 806, 150942. doi:10.1016/j.scitotenv.2021.150942.
- Ghahghaey, Z., Hekmati, M., Darvish Ganji, M., 2021. Theoretical investigation of phenol adsorption on functionalized graphene using DFT calculations for effective removal of organic contaminants from wastewater. *J. Mol. Liq.* 324, 114777. doi:10.1016/J.MOLLIQ.2020.114777.
- Goodwin Jr., D.G., Adeleye, A.S., Sung, L., Ho, K.T., Burgess, R.M., Petersen, E.J., 2018. Detection and quantification of graphene-family nanomaterials in the environment. *Environ. Sci. Technol.* 52 (8), 4491–4513. doi:10.1021/acs.est.7b04938.
- Gupta, K., Khatri, O.P., 2017. Reduced graphene oxide as an effective adsorbent for removal of malachite green dye: Plausible adsorption pathways. *J. Colloid Interface Sci.* 501, 11–21. doi:10.1016/J.JCIS.2017.04.035.
- Huang, C., Li, C., Shi, G., 2012. Graphene based catalysts. *Energy Environ. Sci.* 5, 8848–8868. doi:10.1039/C2EE22238H.
- Ji, J., Yuan, X., Zhao, Y., Jiang, L., Wang, H., 2022. Mechanistic insights of removing pollutant in adsorption and advanced oxidation processes by sludge biochar. *J. Hazard. Mater.* 430, 128375. doi:10.1016/j.jhazmat.2022.128375.
- Ji, L., Chen, W., Xu, Z., Zheng, S., Zhu, D., 2013. Graphene nanosheets and graphite oxide as promising adsorbents for removal of organic contaminants from aqueous solution. *J. Environ. Qual.* 42, 191–198. doi:10.2134/JEQ2012.0172.
- Jiang, L.,hua, Liu, Y.,guo, Zeng, G.ming, Xiao, F.yu, Hu, Xin jiang, Hu, Xi, Wang, H., Li, T.ting, Zhou, L., Tan, X.fei, 2016. Removal of 17 β -estradiol by few-layered graphene oxide nanosheets from aqueous solutions: External influence and adsorption mechanism. *Chem. Eng. J.* 284, 93–102. doi:10.1016/J.CEJ.2015.08.139.
- Jiang, T., Liu, W., Mao, Y., Zhang, L., Cheng, J., Gong, M., Zhao, H., Dai, L., Zhang, S., Zhao, Q., 2015. Adsorption behavior of copper ions from aqueous solution onto graphene oxide–CdS composite. *Chem. Eng. J.* 259, 603–610. doi:10.1016/J.CEJ.2014.08.022.
- Jin, Z., Wang, Xiangxue, Sun, Y., Ai, Y., Wang, Xiangke, 2015. Adsorption of 4-nonylphenol and bisphenol-A on magnetic reduced graphene oxides: a combined experimental and theoretical studies. *Environ. Sci. Technol.* 49, 9168–9175. doi:10.1021/ACS.EST.5B02022/SUPPL_FILE/ESSB02022_SI_001.PDF.
- Kamatchi, R., Venkatachalapathy, S., Srinivas, B.A., 2015. Synthesis, stability, transport properties, and surface wettability of reduced graphene oxide/water nanofluids. *Int. J. Therm. Sci.* 97, 17–25. doi:10.1016/j.ijthermalsci.2015.06.011.
- Kozlov, S.M., Viñes, F., Görling, A., 2012. On the interaction of polycyclic aromatic compounds with graphene. *Carbon* 50, 2482–2492. doi:10.1016/j.carbon.2012.01.070.
- Kumar, P.V., Bardhan, N.M., Tongay, S., Wu, J., Belcher, A.M., Grossman, J.C., 2014. Scalable enhancement of graphene oxide properties by thermally driven phase transformation. *Nat. Chem.* 6, 151–158. doi:10.1038/nchem.1820.
- Kwon, J., Lee, B., 2015. Bisphenol A adsorption using reduced graphene oxide prepared by physical and chemical reduction methods. *Chem. Eng. Res. Des.* 104, 519–529. doi:10.1016/j.cherd.2015.09.007.
- Kyzas, G.Z., Travlou, N.A., Kalogirou, O., Deliyanni, E.A., 2013. Magnetic graphene oxide: effect of preparation route on reactive black 5 adsorption. *Materials* 6, 1360–1376. doi:10.3390/ma6041360.
- Li, M.-s., Wang, R., Fu Kuo, D.T., Shih, Y.-h., 2017. Linear free energy relationships for the adsorption of volatile organic compounds onto multiwalled carbon nanotubes at different relative humidities: comparison with organoclays and activated carbon. *Environ. Sci. Res.* 19 (3), 276–287. doi:10.1039/C6EM00567E.
- Li, T., He, Y., Peng, X., 2020. Efficient removal of tetrabromobisphenol A (TBBPA) using sewage sludge-derived biochar: Adsorptive effect and mechanism. *Chemosphere* 251, 126370. doi:10.1016/j.chemosphere.2020.126370.
- Li, X., Chen, W., Zhang, C., Li, Y., Wang, F., Chen, W., 2016. Enhanced dehydrochlorination of 1,1,2,2-tetrachloroethane by graphene-based nanomaterials. *Environ. Pollut.* 214, 341–348. doi:10.1016/j.envpol.2016.04.035.
- Liu, H., Long, L., Weng, X., Zheng, S., Xu, Z., 2020. Efficient removal of tetrabromobisphenol A using microporous and mesoporous carbons: The role of pore structure. *Micropor. Mesopor. Mat.* 298, 110052. <http://10.1016/j.micromeso.2020.110052>.
- Liu, L., Chen, X., Wang, Z., Wang, X., Lin, S., 2019. The removal mechanism and performance of tetrabromobisphenol A with a novel multi-group activated carbon from recycling long-root *Eichhornia crassipes* plants. *RSC Adv.* 9, 24760–24769. doi:10.1039/C9RA03374B.
- Liu, W.S., Peng, Y.H., Shiung, C.E., Shih, Y.H., 2012. The effect of cations on the aggregation of commercial ZnO nanoparticle suspension. *J. Nanopart. Res.* 14 (12). doi:10.1007/S11051-012-1259-9, doi.org/Artn 1259.
- Louie, S.M., Tilton, R.D., Lowry, G.V., 2016. Critical review: Impacts of macromolecular coatings on critical physicochemical processes controlling environmental fate of nanomaterials. *Environ. Sci.: Nano* 3, 283–310. doi:10.1039/C5EN00104H.
- Lu, L., Wang, J., Chen, B., 2018. Adsorption and desorption of phthalic acid esters on graphene oxide and reduced graphene oxide as affected by humic acid. *Environ. Pollut.* 232, 505–513. doi:10.1016/j.envpol.2017.09.078.
- MacLeod, J.M., Rosei, F., 2011. Directed assembly of nanostructures. *Compr. Nanosci. Technol.* 3 2011, 13–68. doi:10.1016/B978-0-12-374396-1.00098-2.
- Mauter, M.S., Elimelech, M., 2008. Environmental applications of carbon-based nanomaterials. *Environ. Sci. Technol.* 42, 5843–5859. doi:10.1021/es8006904.
- McAllister, M.J., Li, J.-L., Adamson, D.H., Schniepp, H.C., Abdala, A.A., Liu, J., Herrera-Alonso, M., Milius, D.L., Car, R., Prud'homme, R.K., Aksay, I.A., 2007. Single sheet

- functionalized graphene by oxidation and thermal expansion of graphite. *Chem. Mater.* 19, 4396–4404. doi:10.1021/cm0630800.
- Minitha, C.R., Lalitha, M., Jeyachandran, Y.L., Senthilkumar, L., Rajendra Kumar, R.T., 2017. Adsorption behaviour of reduced graphene oxide towards cationic and anionic dyes: Co-action of electrostatic and π - π interactions. *Mater. Chem. Phys.* 194, 243–252. doi:10.1016/j.matchemphys.2017.03.048.
- Mishra, S.K., Tripathi, S.N., Choudhary, V., Gupta, B.D., 2014. SPR based fibre optic ammonia gas sensor utilizing nanocomposite film of PMMA/reduced graphene oxide prepared by in situ polymerization. *Sens. Actuators B* 199, 190–200. doi:10.1016/j.snb.2014.03.109.
- Neelaveni, M., Krishnan, P.S., Ramya, R., Theres, G.S., Shanthi, K., 2019. Montmorillonite/graphene oxide nanocomposite as superior adsorbent for the adsorption of Rhodamine B and Nickel ion in binary system. *Adv. Powder Technol.* 30, 596–609. <http://10.1016/j.apt.2018.12.005>.
- Pei, Z., Li, L., Sun, L., Zhang, S., Shan, X., Yang, S., Wen, B., 2013. Adsorption characteristics of 1,2,4-trichlorobenzene, 2,4,6-trichlorophenol, 2-naphthol and naphthalene on graphene and graphene oxide. *Carbon* 51, 156–163. doi:10.1016/j.carbon.2012.08.024.
- Peng, Y.-H., Tsai, Y.-C., Hsiung, C.-E., Lin, Y.-H., Shih, Y.-h., 2017. Influence of water chemistry on the environmental behaviors of commercial ZnO nanoparticles in various water and wastewater samples. *J. Hazard. Mater.* 322 (Part B), 348–356. doi:10.1016/j.jhazmat.2016.10.003.
- Peng, Y.H., Tso, C.P., Tsai, Y.C., Zhuang, C.M., Shih, Y.H., 2015. The effect of electrolytes on the aggregation kinetics of three different ZnO nanoparticles in water. *Sci. Total Environ.* 530–531, 183–190. doi:10.1016/j.scitotenv.2015.05.059.
- Perumbilavil, S., Sankar, P., Rose, T.P., Philip, R., 2015. White light Z-scan measurements of ultrafast optical nonlinearity in reduced graphene oxide nanosheets in the 400–700 nm region. *Appl. Phys. Lett.* 107, 051104. doi:10.1063/1.4928124.
- Phatthanakitiphong, T., Seo, G.T., 2016. Characteristic evaluation of graphene oxide for bisphenol A adsorption in aqueous solution. *Nanomaterials* 6, 128. doi:10.3390/nano6070128.
- Puga, A., Rosales, E., Sanroman, M.A., Pazos, M., 2020. Environmental application of monolithic carbonaceous aerogels for the removal of emerging pollutants. *Chemosphere* 248, 125995. doi:10.1016/j.chemosphere.2020.125995.
- Qi, Y., Xia, T., Li, Y., Duan, L., Chen, W., 2016. Colloidal stability of reduced graphene oxide materials prepared using different reducing agents. *Environ. Sci.: Nano* 3, 1062–1071. doi:10.1039/C6EN00174B.
- Ren, W., Cheng, H.M., 2014. The global growth of graphene. *Nat. Nanotechnol.* 9, 726–730. doi:10.1038/nnano.2014.229.
- Ren, Y., Abbood, H.A., He, F., Peng, H., Huang, K., 2013. Magnetic EDTA-modified chitosan/SiO₂/Fe₃O₄ adsorbent: Preparation, characterization, and application in heavy metal adsorption. *Chem. Eng. J.* 226, 300–311. doi:10.1016/j.cej.2013.04.059.
- Rout, D.R., Jena, H.M., 2012. Removal of phenol from aqueous solution using reduced graphene oxide as adsorbent: isotherm, kinetic, and thermodynamic studies. *Environ. Sci. Res.* 29, 32105–32119. doi:10.1007/s11356-021-17944-y.
- Rout, P.R., Zhang, T.C., Bhunia, P., Surampalli, R.Y., 2021. Treatment technologies for emerging contaminants in wastewater treatment plants: a review. *Sci. Total Environ.* 753, 141990. doi:10.1016/j.scitotenv.2020.141990.
- Sahu, R.S., Bindumadhavan, K., Doong, R., 2017. Boron-doped reduced graphene oxide-based bimetallic Ni/Fe nanohybrids for the rapid dechlorination of trichloroethylene. *Environ. Sci.: Nano* 4, 565–576. doi:10.1039/C6EN00575F.
- Shen, Y., Fang, Q., Chen, B., 2015. Environmental applications of three-dimensional graphene-based macrostructures: adsorption, transformation, and detection. *Environ. Sci. Technol.* 49, 67–84. doi:10.1021/es504421y.
- Shih, Y.H., Gschwend, P.M., 2009. Evaluating activated carbon-water sorption coefficients of organic compounds using a linear solvation energy relationship approach and sorbate chemical activities. *Environ. Sci. Technol.* 43 (3), 851–857. doi:10.1021/Es801663c.
- Shih, Y.H., Li, M.S., 2008. Adsorption of selected volatile organic vapors on multiwall carbon nanotubes. *J. Hazard. Mater.* 154 (1–3), 21–28. doi:10.1016/j.jhazmat.2007.09.095.
- Shih, Y.H., Su, Y.F., Ho, R.Y., Su, P.H., Yang, C.Y., 2012. Distinctive sorption mechanisms of 4-chlorophenol with black carbons as elucidated by different pH. *Sci. Total Environ.* 433, 523–529. doi:10.1016/j.scitotenv.2012.06.050.
- Shih, Y.H., Su, Y.F., Ho, R.Y., Su, P.H., Yang, C.Y., 2012a. Distinctive sorption mechanisms of 4-chlorophenol with black carbons as elucidated by different pH. *Sci. Total Environ.* 433, 523–529. doi:10.1016/j.scitotenv.2012.06.050.
- Shih, Y.H., Zhuang, C.M., Peng, Y.H., Lin, C.H., Tseng, Y.M., 2012b. The effect of inorganic ions on the aggregation kinetics of lab-made TiO₂ nanoparticles in water. *Sci. Total Environ.* 435, 446–452. doi:10.1016/j.scitotenv.2012.06.076.
- Shih, Y.H., Zhuang, C.M., Tso, C.P., Lin, C.H., 2012c. The effect of electrolytes on the aggregation kinetics of titanium dioxide nanoparticle aggregates. *J. Nanopart. Res.* 14 (8), 924. doi:10.1007/S11051-012-0924-3.
- Sreeprasad, T.S., Pradeep, T., 2012. Graphene for environmental and biological applications. *Int. J. Mod. Phys. B* 26, 1242001. doi:10.1142/S0217979212420015.
- Su, P.-H., Kuo, D.T.F., Shih, Y.-h., Chen, C.-y., 2018. Sorption of organic compounds to two diesel soot black carbons in water evaluated by liquid chromatography and polyparameter linear solvation energy relationship. *Water Res.* 144, 709–718. doi:10.1016/j.watres.2018.07.064.
- Supong, A., Bhomick, P.C., Baruah, M., Pongener, C., Sinha, U.B., Sinha, D., 2019. Adsorptive removal of Bisphenol A by biomass activated carbon and insights into the adsorption mechanism through density functional theory calculations. *Sustain. Chem. Pharm.* 13, 100159. doi:10.1016/j.scp.2019.100159.
- Tene, T., Bellucci, S., Guevara, M., Viteri, E., Polanco, M.A., Salguero, O., Vera-Guzmán, E., Valladares, S., Scarcello, A., Alessandro, F., Caputi, L.S., Gomez, C.V., 2022. Cationic pollutant removal from aqueous solution using reduced graphene oxide. *Nanomaterials* 12, 309. doi:10.3390/nano12030309.
- Tso, C.P., Zhung, C.M., Shih, Y.H., Tseng, Y.M., Wu, S.C., Doong, R.A., 2010. Stability of metal oxide nanoparticles in aqueous solutions. *Water Sci. Technol.* 61 (1), 127–133. doi:10.2166/Wst.2010.787.
- Waiyarat, S., Boontanon, S.K., Boontanon, N., Harrad, S., Abdallah, M.A.-E., Drage, D.S., 2022. Concentrations and human exposure to hexabromocyclododecane and tetrabromobisphenol A from the indoor environment in Bangkok metropolitan area, Thailand. *J. Environ. Expo. Assess.* 1, 11. doi:10.20517/jeea.2022.06.
- Wang, J., Chen, Z., Chen, B., 2014a. Adsorption of polycyclic aromatic hydrocarbons by graphene and graphene oxide nanosheets. *Environ. Sci. Technol.* 48, 4817–4825. doi:10.1021/es405227u.
- Wang, S., Sun, H., Ang, H.M., Tade, M.O., 2013. Adsorptive remediation of environmental pollutants using novel graphene-based nanomaterials. *Chem. Eng. J.* 226, 336–347. doi:10.1016/j.cej.2013.04.070.
- Wang, X., Hu, Y., Min, J., Li, S., Deng, X., Yuan, S., Zuo, X., 2018. Adsorption characteristics of phenolic compounds on graphene oxide and reduced graphene oxide: A batch experiment combined theory calculation. *Appl. Sci.* 8, 1950. doi:10.3390/app8101950.
- Wang, X., Huang, S., Zhu, L., Tian, X., Li, S., Tang, H., 2014b. Correlation between the adsorption ability and reduction degree of graphene oxide and tuning of adsorption of phenolic compounds. *Carbon* 69, 101–112. doi:10.1016/j.carbon.2013.11.070.
- Wu, G., Ma, J., Wang, S., Chai, H., Guo, L., Li, J., Ostovan, A., Guan, Y., Chen, L., 2020. Cationic metal-organic framework based mixed-matrix membrane for extraction of phenoxy carboxylic acid (PCA) herbicides from water samples followed by UHPLC-MS/MS determination. *J. Hazard. Mater.* 394, 122556. doi:10.1016/j.jhazmat.2020.122556.
- Wu, Z., Yuan, X., Zhong, H., Wang, H., Zeng, G., Chen, X., Wang, H., Zhang, L., Shao, J., 2016. Enhanced adsorptive removal of p-nitrophenol from water by aluminum metal-organic framework/reduced graphene oxide composite. *Sci. Rep.* 6, 25638. doi:10.1038/srep25638.
- Xie, B., Qin, J., Wang, S., Li, X., Sun, H., Chen, W., 2020. Adsorption of phenol on commercial activated carbons: Modelling and interpretation. *Int. J. Environ. Res. Public Health* 17, 789. doi:10.3390/ijerph17030789.
- Xu, J., Wang, L., Zhu, Y., 2012. Decontamination of bisphenol A from aqueous solution by graphene adsorption. *Langmuir* 28, 8418–8425. doi:10.1021/la301476p.
- Yan, H., Tao, X., Yang, Z., Li, K., Yang, H., Li, A., Cheng, R., 2014. Effects of the oxidation degree of graphene oxide on the adsorption of methylene blue. *J. Hazard. Mater.* 268, 191–198. doi:10.1016/j.jhazmat.2014.01.015.
- Yan, H., Wu, H., Li, K., Wang, Y., Tao, X., Yang, H., Li, A., Cheng, R., 2015. Influence of the surface structure of graphene oxide on the adsorption of aromatic organic compounds from water. *ACS Appl. Mater. Interfaces* 7, 6690–6697. doi:10.1021/acsami.5b00053.
- Yang, S., Wang, S., Sun, F., Zhang, M., Wu, F., Xu, F., Ding, Z., 2015. Protective effects of puerarin against tetrabromobisphenol A-induced apoptosis and cardiac developmental toxicity in zebrafish embryo-larvae. *Environ. Toxicol.* 30, 1014–1023. doi:10.1002/tox.21975.
- Yu, S., Wang, X., Ai, Y., Tan, X., Hayat, T., Hu, W., Wang, X., 2016. Experimental and theoretical studies on competitive adsorption of aromatic compounds on reduced graphene oxides. *J. Mater. Chem.* 4, 5654–5662. doi:10.1039/C6TA00890A.
- Yu, S., Wang, X., Yao, W., Wang, J., Ji, Y., Ai, Y., Alsaedi, A., Hayat, T., Wang, X., 2017. Macroscopic, spectroscopic, and theoretical investigation for the interaction of phenol and naphthol on reduced graphene oxide. *Environ. Sci. Technol.* 51, 3278–3286. doi:10.1021/acs.est.6b06259.
- Zhang, W., Chen, J., Hu, Y., Fang, Z., Cheng, J., Chen, Y., 2018. Adsorption characteristics of tetrabromobisphenol A onto sodium bisulfite reduced graphene oxide aerogels. *Colloids Surf. A* 538, 781–788. doi:10.1016/j.colsurfa.2017.11.070.
- Zhang, Y., Adams, R.D., da Silva, L.F.M., 2014. Absorption and glass transition temperature of adhesives exposed to water and toluene. *Int. J. Adhes. Adhes.* 50, 85–92. doi:10.1016/j.ijadhadh.2014.01.022.
- Zhang, Y., Tang, Y., Li, S., Yu, S., 2013. Sorption and removal of tetrabromobisphenol A from solution by graphene oxide. *Chem. Eng. J.* 222, 94–100. doi:10.1016/j.cej.2013.02.027.